Image transfer by cascaded stack of photonic crystal and air layers

C. Shen, K. Michielsen, H. De Raedt

Department of Applied Physics, Materials Science Centre, University of Groningen,
Nijenborgh 4, NL-9747 AG Groningen, The Netherlands

h.a.de.raedt@rug.nl

http://www.compphys.org

Abstract: We demonstrate image transfer by a cascaded stack consisting of two and three triangular-lattice photonic crystal slabs separated by air. The quality of the image transfered by the stack is sensitive to the air/photonic crystal interface termination and the frequency. Depending on the frequency and the surface termination, the image can be transfered by the stack with very little deterioration of the resolution, that is the resolution of the final image is approximately the same as the resolution of the image formed behind one single photonic crystal slab.

OCIS codes: (260.2110) Electromagnetic theory; (110.2990) Image formation theory; (120.5710) Refraction; (220.3630) Lenses; (999.9999) Photonic crystals.

References and links

1. A. Bers, "Note on group velocity and energy propagation", Am. J. Phys. **68**, 482 – 484 (2000).
2. J.B. Pendry and D.R. Smith, "Reversing light with negative refraction," Phys. Today **57**, 37 – 43 (2004).
3. S. Foteinopoulou, E.N. Economou, and C.M. Soukoulis, "Refraction in media with a negative refractive index," Phys. Rev. Lett. **90**, 107402 (2003).
4. J.B. Brock, A.A. Houck, and I.L. Chuang, "Focusing inside negative index materials," Appl. Phys. Lett. **85**, 2472 – 2474 (2004).
5. V.G. Veselago, "The electrodynamics of substances with simultaneously negative values of ε and μ," Sov. Phys. Usp. **10,** 509 – 514 (1968). [Translation from the original Russion version in Usp. Fiz. Nauk. **92,** 517 – 526 (1967). This year was mislabeled in the translation as 1964.].
6. R.W. Ziolkowski, "Wave propagation in media having negative permittivity and permeability," Phys. Rev. E **64**, 056625 (2001).
7. R.W. Ziolkowski, "Pulsed and CW Gaussian beam interactions with double negative metamaterial slabs," Opt. Express **11**, 662 – 681 (2003), http://www.opticsexpress.org/abstract.cfm?URI=OPEX-11-7-662.
8. I.V. Lindell, S.A. Tretyakov, K.I. Nikoskinen, and S. Ilvonen, "BW media- media with negative parameters, capable of supporting backward waves," Microw. Opt. Tech. Lett. **31**, 129 – 133 (2001).
9. I.V. Lindell and S. Ilvonen, "Waves in a slab of uniaxial BW medium," J. of Electromagn. Waves and Appl. **16**, 303 – 318 (2002).
10. R.G.E. Hutter, *Beam and wave electronics in microwave tubes*, (Van Nostrand, Princeton, NJ, 1960), p.220.
11. P.E. Mayes, G.A. Deschamps, and W.T. Patton, "Backward-wave radiation from periodic structures and application to the design of frequency-independent antennas," Proc. IRE **49**, 962 – 963 (1961).
12. J.L. Altman, *Microwave circuits*, (Van Nostrand, Princeton, NJ, 1964), chap.7, p.304.
13. R.E. Collin, *Foundations for vmicrowave engineering*, (McGraw-Hill, New York, 1966).
14. A.A. Oliner and T. Tamir, "Backward waves on isotropic plasma slabs," J. Appl. Phys. **33**, 231 – 233 (1962).
15. http://www.wave-scattering.com/negative.html.
16. H. Lamb, "On group-velocity," Proc. London Math. Soc. **1**, 473 – 479 (1904).
17. H.C. Pocklington, "Growth of a wave-group when the group-velocity is negative," Nature **71**, 607 – 608 (1905).
18. R.A. Silin, "Possibility of creating plane-parallel lenses," Opt. Spectrosc. (USSR) **44**, 109 – (1978). [Translation from the original Russian version in Opt. Spektrosk. **44**, 189 – 191 (1978).]

19. J.B. Pendry, "Negative refraction makes a perfect lens," Phys. Rev. Lett. **85,** 3966 – 3969 (2000).
20. P.F. Loschialpo, D.L. Smith, D.W. Forester, F.J. Rachford, and J. Schelleng, "Electromagnetic waves focused by a negative-index planar lens," Phys. Rev. E **67**, 025602 (2003).
21. P.F. Loschialpo, D.W. Forester, D.L. Smith, F.J. Rachford, and C. Monzon, "Optical properties of an ideal homogeneous causal left-handed material slab," Phys. Rev. E **70**, 036605 (2004).
22. M. Notomi, "Theory of light propagation in strongly modulated photonic crystals: Refractionlike behavior in the vicinity of the photonic band gap," Phys. Rev. B **62,** 10696 – 10705 (2000).
23. A. Berrier, M. Mulot, M. Swillo, M. Qiu, L. Thylén, A. Talneau, and S. Anand, "Negative refraction at infrared wavelengths in a two-dimensional photonic crystal," Phys. Rev. Lett. **93,** 073902 (2004).
24. A. Martinez, H. Miguez, A. Griol, and J. Marti, "Experimental and theoretical analysis of the self-focusing of light by a photonic crystal lens," Phys. Rev. B **69,** 165119 (2004).
25. K. Guven, K. Aydin, K.B. Alici, C.M. Soukoulis and E. Ozbay, "Spectral negative refraction and focusing analysis of a two-dimensional left-handed photonic crystal lens," Phys. Rev. B **70,** 205125 (2004).
26. E. Ozbay, I. Bulu, K. Aydin, H. Caglayan, K.B. Alici, and K. Guven, "Highly directive radiation and negative refraction using photonic crystals," Laser Phys. **15,** 217 – 224 (2005).
27. M. Notomi, "Negative refraction in photonic crystals," Opt. Quant. Electr. **34,** 133 – 143 (2002).
28. X. Wang, Z.F. Ren, and K. Kempa, "Unrestricted superlensing in a triangular two dimensional photonic crystal," Opt. Express **12,** 2919 – 2924 (2004), http://www.opticsexpress.org/abstract.cfm?URI=OPEX-12-13-2919.
29. S. Xiao, M. Qiu, Z. Ruan, S. He, "Influence of the surface termination to the point imaging by a photonic crystal slab with negative refraction," Appl. Phys. Lett. **85,** 4269 – 4271 (2004).
30. X. Zhang, "Image resolution depending on slab thickness and object distance in a two-dimensional photonic-crystal-based superlens," Phys. Rev. B **70,** 195110 (2004).
31. X. Wang and K. Kempa, "Effects of disorder on subwavelength lensing in two-dimensional photonic crystal slabs," Phys. Rev. B **71,** 085101 (2005).
32. X. Wang, Z.F. Ren, and K. Kempa, "Improved superlensing in two-dimensional photonic crystals with a basis," Appl. Phys. Lett. **86,** 061105 (2005).
33. A. Martinez and J. Marti, "Analysis of wave focusing inside a negative-index photonic-crystal slab," Opt. Express **13,** 2858 –2868 (2005), http://www.opticsexpress.org/abstract.cfm?URI=OPEX-13-8-2858.
34. C. Luo, S.G. Johnson, J.D. Joannopoulos, J.B. Pendry, "All-angle negative refraction without negative effective index," Phys. Rev. B **65,** 201104 (2002).
35. S. He and Z. Ruan, "A completely open cavity realized with photonic crystal wedges," J. Zhejiang Univ. SCI **6**A, 355 – 357 (2005).
36. Z. Ruan and S. He, "Open cavity formed by a photonic crystal with negative effective index of refraction," Opt. Lett. **30,** 2308 – 2310 (2005).
37. S. He, Y. Jin, Z. Ruan, and J. Kuang, "On subwavelength and open resonators involving metamaterials of negative refraction index," New Journal of Physics **7,** 210 (2005).
38. J.S. Kole, M.T. Figge, and H. De Raedt, "Unconditionally stable algorithms to solve the time-dependent Maxwell equations," Phys. Rev. E **64,** 066705 (2001).
39. A. Taflove and S.C. Hagness, *Computational Electrodynamics: The Finite-Difference Time-Domain Method*, 3rd edition, (Artech House, MA USA, 2005).
40. S.G. Johnson and J.D. Joannopoulos, "Block-iterative frequency-domain methods for Maxwell's equations in a planewave basis," Opt. Express **8,** 173 – 190 (2001), http://www.opticsexpress.org/abstract.cfm?URI=OPEX-8-3-173.
41. Z. Ruan, M. Qiu, S. Xiao, S. He, and L. Thylén, "Coupling between plane waves and Bloch waves in photonic crystals with negative refraction," Phys. Rev. B **71,** 045111 (2005).

1. Introduction

For homogeneous, isotropic dielectric media with simultaneously negative permittivity $\varepsilon(\mathbf{r})$ and permeability $\mu(\mathbf{r})$, the electric field vector $\mathbf{E}(\mathbf{r})$, the magnetic field vector $\mathbf{H}(\mathbf{r})$ and the wave vector $\mathbf{k}$ form a left-handed set of vectors. The Poynting vector $\mathbf{S}$ always forms a right-handed set with the vectors $\mathbf{E}$ and $\mathbf{H}$. Accordingly, $\mathbf{S}$ and $\mathbf{k}$ are antiparallel, that is $\mathbf{S} \cdot \mathbf{k} < 0$. In weakly dispersive media, the group velocity $\mathbf{v}_g$ identifies the direction of energy propagation, that is $\mathbf{S} \cdot \mathbf{v}_g > 0$ [1], hence the sign of $\mathbf{v}_g \cdot \mathbf{k}$ is equivalent to the sign of $\mathbf{S} \cdot \mathbf{k}$, which in this case is negative. The group velocity is called negative, that is having the opposite sign of the wave vector. The sign of the refractive index n is the sign of $\mathbf{S} \cdot \mathbf{k}$ and thus also of $\mathbf{v}_g \cdot \mathbf{k}$. Thus, homogeneous isotropic dielectric media with simultaneously negative ε and μ have a negative refractive index. Therefore, these materials are often called negative index materials (NIMS) (see for example Refs. [2–4]). However, several other names are also used in the

literature. Veselago referred to these materials as left-handed materials [5], Ziolkowski *et al.* denoted these materials as double negative materials [6, 7] and Lindell *et al.* suggested the name backward-wave media [8, 9]. They were however not the first to use this name. Already at the end of the fifties and the beginning of the sixties backward waves were known to exist in some periodic structures with applications to microwave amplifiers, oscillators and antennas [10–13]. Backward-waves have also been generated in continuous structures like a sheet of plasma [14]. However, as mentioned on the website of Moroz [15], Lamb and Schuster in 1904 may even have been the first to study the possibility of a negative group velocity, that is having the opposite sign to the wave vector, and thus to study the existence of backward waves. Lamb studied mechanical systems, free from dissipation, in which the group velocity can become negative [16]. In his paper, Lamb mentioned that Schuster proposed to him the possibility of a negative group velocity and that Schuster pointed out that the optical formulae relating to anomalous dispersion indicate a negative group velocity for certain portions of the spectrum lying within the regions of special absorption. Also Pocklington mentioned in 1905 waves propagating toward the source of disturbance in a mechanical system [17].

One of the interesting properties of NIMs is their ability to focus light. In 1967, Veselago pointed out that a flat plate of thickness D made of a NIM with refractive index $\hat{n} = -1$ and situated in vacuum ($n = 1$) can focus radiation from a point source P positioned at a distance $L < D$ from one side of the plate to a point P' located at a distance $L' = D - L$ from the other side of the plate [5]. An image inside the slab as well as an image outside the slab is formed. In 1978, Silin showed that plane-parallel lenses can be constructed on the basis of media with negative dispersion [18]. He demonstrated that it is possible to choose an isotropic medium such that monochromatic aberrations can be eliminated from such lenses [18]. In 2000, Pendry further pointed out that flat slabs of NIM with $\hat{n} = -1$ and surrounded by vacuum make perfect lenses or superlenses, since both propagating and evanescent waves contribute to the resolution of the image [19]. Those lenses are thus predicted to have subwavelength resolution. As a result, a lot of research has been performed on NIMs and superlenses since 2000. However, limitations of the superlensing effect have also been subject of debate. In 2001, Ziolkowski *et al.* have shown analytically that the perfect lens effect exists only for a NIM with $\varepsilon = \mu = -1$ that is both lossless and nondispersive [6]. The perfect lens effect was shown not to exist for anay realistic dispersive, lossy NIM. The simulation results of Loschialpo *et al.* [20, 21] do not support a perfect lens, as postulated by Pendry [19], either.

In 2000, Notomi has shown theoretically that photonic crystals (PhCs), periodic dielectric composite structures with an electric permittivity $\varepsilon > 0$ and a magnetic permeability $\mu = 1$, near the bandgap frequency behave as if they have an effective refractive index [22]. For some frequency regions this effective refractive index can be negative [22]. As a result, in these frequency regions, PhCs can exhibit similar phenomena as observed in NIMs, including negative refraction and imaging by a planar surface [22]. Imaging effects have been demonstrated experimentally [23–26] as well as theoretically [22, 24–33] for triangular-lattice PhCs. These PhCs can have a negative effective refractive index, as seen from the equifrequency surfaces (EFSs) [22]. Also for square-lattice PhCs, imaging effects have been reported, but these PhCs do not have a negative effective refractive index [34].

Besides imaging by a flat lens, Notomi mentioned two other applications of NIMs: Open cavity formation [22, 27] and image transfer by a cascaded stack of alternatingly positioned, positive and negative refractive media [27]. Recently, an open cavity formed by three 60-degree wedges of a PhC with a negative effective refractive index has been designed and studied [35–37]. In this paper we present the first study of image transfer by a cascaded stack consisting of two and three two-dimensional PhC slabs separated by air.

2. Numerical method

The cascaded stack is illuminated by a point source located at $\mathbf{r} = \mathbf{r}_0$ and modeled by

$$\mathbf{J}(\mathbf{r},t) = \mathbf{n}\theta(t)\delta(\mathbf{r} - \mathbf{r}_0)\sin\omega t, \qquad (1)$$

where $\mathbf{n}$ defines the direction of the electric current (TM-mode) and ω is the angular frequency of the source. The point source is placed in front of the stack at a distance L from the most left air/PhC interface. The location of the source is chosen such that it is located at one of the E_z-points of the two-dimensional Yee grid (TM-mode). As indicated by the step function in Eq. (1), the source is turned on at $t = 0$. In order to study the imaging properties of the cascaded stack we solve the time-dependent Maxwell equations (TDME) by means of a finite-difference time-domain method that, in the absence of external currents, conserves the energy exactly [38, 39]. We first let the system evolve in time until a stationary state is reached and then we average the electric field intensity over one period $2\pi/\omega$. We study the image quality from the electric field intensity distribution, plotted along the image center perpendicular (along the x-axis) and parallel (along the y-axis) to the air/PhC slab interfaces. The corresponding longitudinal and transversal spatial resolutions, defined as the ratio of the full width at half maximum (FWHM) to the wavelength λ of the light, are R_x and R_y, respectively. For reference, and because it is most frequently shown in the current literature, we also show the electric field amplitude.

In our numerical work, we use rectangular simulation areas having boundaries that are absorbing. We measure distances in units of the wavelength λ of light in vacuum. Time and frequency are then expressed in units of λ/c and c/λ, respectively, where c denotes the velocity of light in vacuum. For PhCs with lattice constant a, $f = \omega a/(2\pi c)$ is the dimensionless frequency. We employ a square grid with lattice spacing $\delta = 0.01\lambda$. We solve the TDME using a fourth-order unconditionally stable algorithm [38] with a time step $\delta t = 0.001\lambda/c$. Smaller values for the lattice spacing δ and the time step δt give similar results as the ones presented in this paper.

3. Parameters of the photonic crystal slabs

We consider PhC slabs made of a triangular lattice of air holes, drilled in a dielectric material with $\varepsilon = 12.96$, $\mu = 1$. The holes have a radius $r = 0.4a$. We use the MIT Photonic-Bands (MPB) package [40] to compute the photonic band structure diagram and the EFSs. For the dimensionless frequency range $f = \omega a/2\pi c = 0.26 - 0.33$, corresponding to frequencies in band two, the EFS plot for the TM mode is depicted in the left panel of Fig. 1. For some frequencies, the shape of the EFS is circular. In this case, we can extract an effective refractive index $\hat{n}$ from the radius of the EFS using Snell's law [22]. The sign of $\hat{n}$ is determined by the behavior of the EFSs as a function of f. From Fig. 1 it can be seen that the EFSs move inwards with increasing frequency. Hence, $\hat{n} < 0$ ($\mathbf{v}_g \cdot \mathbf{k} < 0$) [22]. The effective refractive index $\hat{n}$ as a function of the angle θ of the incoming wave vector $\mathbf{k}$ is shown in the right panel of Fig. 1. For $f = 0.3$, $\hat{n}$ is almost independent of θ and is almost equal to -1. Small changes in f lead to large changes in $\hat{n}$.

Light propagating through a homogeneous isotropic slab with $\hat{n} = -1$ embedded in air is not reflected at the air/slab interfaces. For a slab made of a PhC with an effective refractive index of $\hat{n} = -1$ the transmission of light is not 100% and strongly depends on the orientation of the PhC and on the terminations of the air/slab interfaces. Transmission is maximal if the surface normal of the slabs is along the ΓM direction [41] and if the air holes at the air/PhC interfaces are cut [29, 31]. We therefore consider PhC slabs consisting of N layers of air spheres with cutted air/PhC interfaces normal to the ΓM direction. Simulation results for PhC slabs with $N = 9$ indicate that images with the best spatial resolutions R_x and R_y are obtained if the
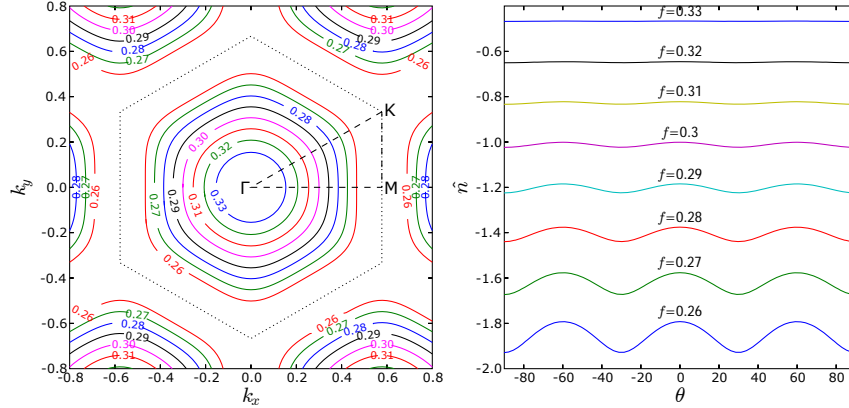
Fig. 1. Left: Equifrequency surface plot of TM modes for a triangular lattice photonic crystal consisting of air holes with a radius of $r = 0.4a$, drilled in a dielectric medium ($\varepsilon = 12.96$, $\mu = 1$) for the frequency range $f = 0.26 - 0.33$. The first Brillouin zone of a triangular lattice (dotted line) and the symmetry points are also shown. Right: Effective refractive index $\hat{n}$ as a function of the angle θ of the incoming wave vector $\mathbf{k}$ for the frequency range $f = 0.26 - 0.33$.

cutted area at both air/PhC interfaces has a width $C = 0.5r$ (results not shown). Concerning the maximum of the transmitted intensity (maximum of the intensity behind the slab), $C = 0.3r$ is a slightly better choice than $C = 0.5r$. Because the maximum of the transmitted intensity is low anyway (5.2% for $C = 0.3r$ compared to 3.8% for $C = 0.5r$, if we normalize the maximum of the source intensity to 100%), we only consider PhC slabs with $C = 0.5r$. Hence, the thickness of the slabs is given by $D = (N-1)\sqrt{3}a/2 + 0.4a$.

4. Image transfer by a cascaded stack

A flat plate of thickness D made of NIM with $\hat{n} = -1$ and situated in vacuum can focus radiation from a point source P positioned at a distance $L < D$ from one side of the plate to a point P' located at a distance $L' = D - L$ from the other side of the plate [5]. Also inside the plate an image is formed. Due to the relation $L + L' = D$, the distance between P and P' is always equal to $2D$. Hence, to increase the distance between P and P' there are two possibilities: Increasing D or applying the principle of image transfer by a cascaded stack. If the flat plates are made of a PhC with an effective refractive index $\hat{n} = -1$, only one option is feasible: Taking one PhC slab and increasing its thickness leads to worsening spatial resolutions of the image that is formed behind the slab.

In order to have PhC slabs with $\hat{n} \approx -1$, we consider a source, emitting TM waves with a frequency $f = 0.299$. We first consider a cascaded stack composed of two PhC slabs with thickness $D = 6.33\lambda$ ($N = 25$). The slabs are separated by an air layer of thickness 6.43λ. The source is placed at a distance $L = 3.29\lambda$ from the left surface of the first PhC slab. Figure 2 depicts the electric field intensity and amplitude. The material structure of the PhC slab is not shown in order to give a better image of the light focusing inside the slabs. The lines indicate the direction of propagation according to Snell's law for the case of a homogeneous isotropic slab with $\hat{n} = -1$. From Fig. 2 it can be seen that there is a relatively good agreement between our simulation results and the results obtained from the rules of geometric optics. Light focusing occurs inside the slabs, in between the two slabs and behind the two slabs. The focus behind the two slabs is not circular, but elongated in the direction of propagation. This has also been
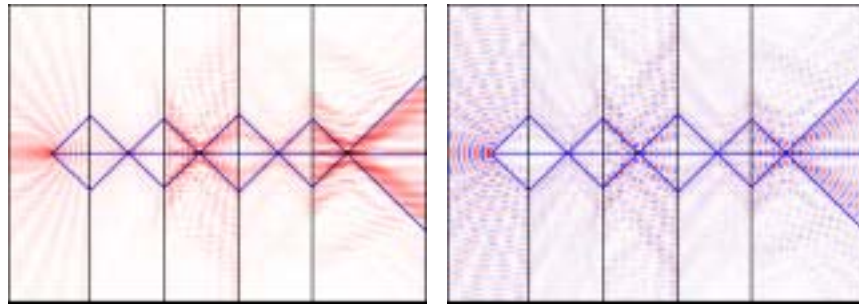
Fig. 2. Left: Intensity of the electric field of a TM wave with frequency $f = 0.299$, generated by a point source placed in front of a cascaded stack composed of two PhC slabs with an air layer in between. For the description of the imaging system we refer to the text. The blue lines indicate the propagation directions according to Snell's law for a homogeneous slab with $\hat{n} = -1$. Intensities are plotted on a $\log_{10}$ scale. The field intensities are scaled between 0 and 1. Because the transmitted intensity is low, the intensities are scaled different for the regions to the left of the stack, in between the slabs, behind the stack and inside the slabs. Right: Amplitude of the electric field. The electric field amplitudes are plotted on a linear scale ranging from -1 to +1 (blue: Negative values, red: Positive values) and are scaled different for the regions to the left of the stack, in between the slabs, behind the stack and inside the slabs.

observed in previous works for single slab imaging [25, 30, 33] and is due to slight deviations of $\hat{n}$ from -1 for different angles of incidence. Hence, we do not observe point focusing and in a strict sense, there is no image formation. However, we can say we observe image formation with some aberrations. The spatial resolutions of the image behind the second slab are $R_x = 1.76$ and $R_y = 0.46$. As can be clearly seen from the left panel of Fig. 2, this image is different from the image in between the two slabs. However, if we remove the second slab and repeat the same calculation, then an image with the same spatial resolutions is formed (results not shown). Hence, the first image (behind the first slab) is transfered through the second slab, so that the second image (behind the second slab) is a copy of the first image. The first image gets distorted by reflections from the second slab. This would not happen in the ideal case, that is in the case of two slabs made of a homogeneous isotropic material with $\hat{n} = -1$. Note that the picture of the electric field amplitude (see right panel of Fig. 2) suggests a more circular image that is transfered by the cascaded stack and thus better imaging properties of the slabs. However, the picture of the electric field amplitude displays only a snapshot. Moreover, it is not sufficient to study field amplitudes in order to investigate the imaging properties of a PhC system since they cannot be measured directly.

The imaging properties of the cascaded stack are very sensitive to the frequency of the source and the surface terminations of the PhC slabs. The left panel of Fig. 3 shows the electric field intensity for the same setup as the one that was used to obtain the results displayed in Fig. 2 but for the frequency $f = 0.300$. For this frequency images are also formed inside the slabs, in between the two slabs and behind the two slabs, but the deviations from propagation through a homogeneous isotropic slab with $\hat{n} = -1$ is much larger than for $f = 0.299$, as indicated by the propagation lines obtained from Snell's law. Moreover, the image formed behind the two slabs is no longer an exact copy of the image formed behind the first slab. The spatial resolution changes from $R_x = 1.60$, $R_y = 0.42$ for the first image to $R_x = 1.70$, $R_y = 0.42$ for the second image. Hence, for this particular case, additional longitudinal aberrations are induced by the
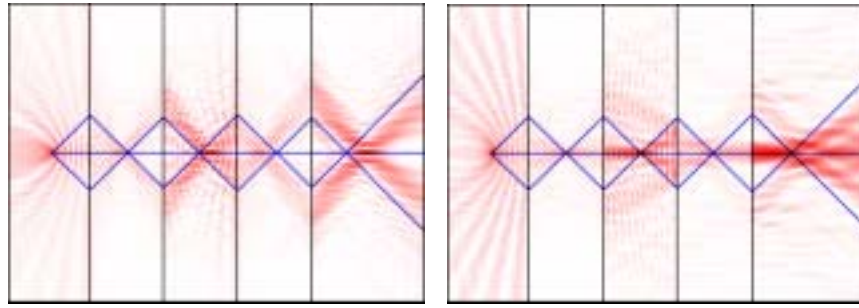
Fig. 3. Same as the left panel of Fig. 2 for $f = 0.300$ (left) and for air/PhC interfaces that are not cut (right).

second slab. Note however, that the spatial resolutions of the image formed behind the second slab in Fig. 3 (left panel) are better than the ones of the image formed behind the second slab in Fig. 2 (left panel). The right panel of Fig. 3 shows the electric field intensity for the same setup as the one that was used to obtain the results displayed in Fig. 2 but the air/PhC interfaces of the slabs are not cut. It is clearly seen that in this case, no image transfer by the cascaded stack can be observed.

Another important issue is the intensity of the images. If we normalize the maximum of the source intensity to 100%, then, for the case studied in Fig. 2, the intensity maximum in the first slab corresponds to 7.7%, in between the two slabs to 1.8%, inside the second slab to 1.7% and behind the second slab to 0.7%. Similar simulation results for a cascaded stack with two PhC slabs with $N = 15$, show that the intensity maximum in the first slab corresponds to 7.0%, in between the two slabs to 3.8%, inside the second slab to 2.6% and behind the second slab to 1.3%. Hence, even for cascaded stacks with thin PhC slabs the maximum of the transmitted intensity is rather low. This observation is in agreement with the observation that the maximum coupling coefficient between a plane wave in air and the Bloch wave in the PhC is only about 65% and rapidly decreases for angles of incidence larger than 30°, for an air/PhC interface normal to the ΓM direction [41]. Additional simulations (results not shown) show that the intensity in the images depends on the thickness of the slabs, the frequency and the size of the cutted area at the surface terminations. However, for all cases studied the intensities were of the same order as mentioned before.

In order to investigate the dependence of the maxima of the transmitted intensity on the number of slabs in the stack, we consider a cascaded stack composed of three PhC slabs with thickness $D = 3.74\lambda$ ($N = 15$). The PhC slabs are separated by air layers of the same thickness as the slabs. The source is placed at a distance $L = 1.87\lambda$ from the left surface of the first PhC slab. Figure 4 depicts the electric field intensity. The intensity maximum in the first slab corresponds to 6.6%, in between slab 1 and slab 2 to 3.6%, in the second slab to 3.3%, in between slab 2 and 3 to 1.5%, in the third slab to 1.6% and behind the third slab to 0.7%. Hence, for cascaded stacks with three PhC layers with $N = 15$, our simulations show that the maximum of the intensity behind the last slab decreases, compared to the case of a cascaded stack with only two PhC slabs: For three slabs, the maximum of the intensity behind the last slab corresponds to 0.7%, while for the two slab case it corresponds to 1.3%, as shown before. Similar simulations with one single slab show that for a single slab the maximum of the transmitted intensity corresponds to 3.4%. These results indicate that each slab that is added to the stack reduces the intensity by a factor of two. In this particular case, additional longitudinal aberrations are
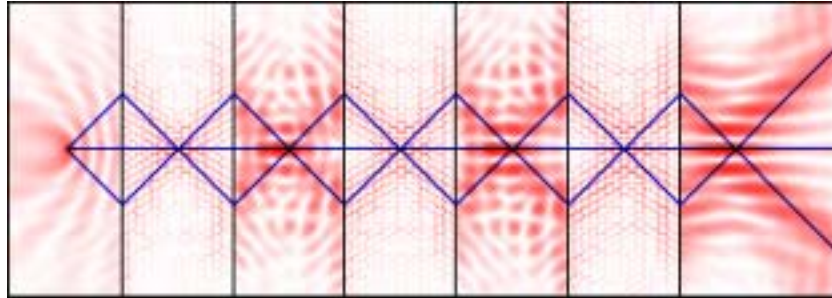
Fig. 4. Same as the left panel of Fig. 2 for a cascaded stack with three PhC slabs. For the description of the imaging system we refer to the text.

induced by each slab that is added to the stack. The transversal spatial resolution of the image remains approximately the same upon transfer of the image through the stack.

5. Summary and conclusions

In order to increase the source/image distance in flat slab imaging, which is limited to two times the thickness of the slab, one could use one thick slab or a cascaded stack consisting of several thinner slabs separated by air. If the slabs are made of a photonic crystal material, using one thick slab is not an option, since the image resolution becomes worse as the thickness increases. In this paper we have demonstrated the working principle of image transfer by a cascaded stack consisting of two and three photonic crystal slabs separated by air. The quality of the image transfered by the stack and the maximum of the transmitted intensity depends on the frequency of the light, the thickness of the photonic crystal slabs, the surface termination of the photonic crystal slabs and on the distance between the slabs. Although the transmitted intensity is rather low for cascaded stacks consisting of two photonic crystal slabs, it seems that more slabs can be added without a further significant decrease of the intensity. The image transfer over a given distance requires the solution of an optimization problem, involving the number of slabs in the stack, the thickness of the slabs, the distance between the slabs and the frequency of the light.

Acknowledgments